

Self-Assembly and Hydrogelation of an Amyloid Peptide Fragment

Marta J. Krysmann,[‡] Valeria Castelletto,[‡] Antonios Kelarakis,^{‡,§} Ian W. Hamley,^{*,‡} Rohan A. Hule,^{II} and Darrin J. Pochan^{II}

Department of Chemistry, University of Reading, Reading RG6 6AD, United Kingdom, and Department of Materials Science and Engineering, Delaware Biotechnology Institute, University of Delaware, Newark, Delaware 19716

Received January 11, 2008; Revised Manuscript Received February 18, 2008

ABSTRACT: The self-assembly of a fragment of the amyloid β peptide that has been shown to be critical in amyloid fibrillization has been studied in aqueous solution. There are conflicting reports in the literature on the fibrillization of $A\beta$ (16–20), i.e., KLVFF, and our results shed light on this. In dilute solution, self-assembly of NH_2 –KLVFF–COOH is strongly influenced by aromatic interactions between phenylalanine units, as revealed by UV spectroscopy and circular dichroism. Fourier transform infrared (FTIR) spectroscopy reveals β -sheet features in spectra taken for more concentrated solutions and also dried films. X-ray diffraction and cryo-transmission electron microscopy (cryo-TEM) provide further support for β -sheet amyloid fibril formation. A comparison of cryo-TEM images with those from conventional dried and negatively stained TEM specimens highlights the pronounced effects of sample preparation on the morphology. A comparison of FTIR data for samples in solution and dried samples also highlights the strong effect of drying on the self-assembled structure. In more concentrated phosphate-buffered saline (PBS) solution, gelation of NH_2 –KLVFF–COOH is observed. This is believed to be caused by screening of the electrostatic charge on the peptide, which enables β sheets to aggregate into a fibrillar gel network. The rheology of the hydrogel is probed, and the structure is investigated by light scattering and small-angle X-ray scattering.

The formation of amyloid because of misfolding of proteins and peptides is symptomatic of diseases including Alzheimer's, bovine spongiform encephalopathy, etc. (1–6). Amyloid results from fibrillization as peptides adopt a cross- β -sheet structure, with β strands perpendicular to the long fibril axis. The amyloid β peptide ($A\beta$)¹ undergoes fibrillization and forms amyloid deposits *in vivo*. The peptide is enzymatically cleaved from the amyloid precursor protein to produce fragments with primarily 40 or 42 residues, $A\beta$ 40 and $A\beta$ 42, respectively (6).

The fibrillization of several fragments of $A\beta$ has been investigated by a number of groups. Early work has been reviewed elsewhere (1, 7). The results of experimental and modeling work by several groups (8–21) suggests that sequence $A\beta$ (16–20), i.e., KLVFF, is critical for fibrillization. In the following, we review some of the key studies that led to this finding. Hilbich et al. showed that a region in the hydrophobic core around residues 17–20, i.e., LVFF, is crucial for β -sheet formation (8). They prepared variants of

$A\beta$ 43, with substitution of various residues 17–20 and investigated fibrillization by circular dichroism (CD), Fourier transform infrared (FTIR), and transmission electron microscopy (TEM). Substitution with hydrophilic amino acids led to a significant reduction in amyloid formation. Tjernberg et al. studied the binding of fragments and variant fragments of $A\beta$ 40 to the full peptide (10, 11). A series of fragments of $A\beta$ 40 ranging from 3 to 10 residues was prepared. Only pentapeptides or longer showed significant binding to $A\beta$ 40, and fragment $A\beta$ (16–20), i.e., KLVFF, is contained in all strongly binding sequences (11). When pentapeptide variants of KLVFF were prepared with substituted amino acids, it was found that residues 2, 3, and 5 (K, L, and F) are most important for binding of this fragment to $A\beta$ 40 (10, 11).

The dependence of fibrillization on fragment size was investigated for $A\beta$ fragments containing the $A\beta$ (16–20) sequence (12). Electron microscopy suggested that the shortest fibril-forming sequence was $A\beta$ (14–23), i.e., the decapeptide HQKLVFFAED. The KLVFF sequence was found not to form fibrils itself. Meredith and co-workers later studied variants of KLVFF (15) and KLVFFAE (14), in which amide protons in alternate residues were replaced by *N*-methyl groups (14, 15). These fragments are believed to form β strands with distinct faces: one with unmodified groups capable of forming hydrogen bonds and the other containing nonpolar methyl groups. This can disrupt the hydrogen-bonded β -sheet structure of the $A\beta$ peptide itself.

TEM indicated that KLVFF itself forms fibrils in aqueous phosphate-buffered saline (PBS) solutions (pH 7.4) (15), contrary to the reports by Tjernberg et al. (12). There is therefore some controversy as to whether this fragment itself

* To whom correspondence should be addressed: also at Diamond Light Source, Didcot, Oxfordshire OX11 0DE, U.K. Telephone: +44-118-378-8453. Fax: +44-118-378-6331. E-mail: i.w.hamley@reading.ac.uk.

[‡] University of Reading.

[§] Current address: National and Kapodistrian University of Athens, Department of Chemistry, Physical Chemistry Laboratory, Panepistimiopolis, 157 71 Athens, Greece.

^{II} University of Delaware.

¹ Abbreviations: $A\beta$, amyloid β peptide; CD, circular dichroism; cryo-TEM, cryogenic transmission electron microscopy; FTIR, Fourier transform infrared; MALDI–TOF, matrix-assisted laser desorption/ionization time-of-flight; SAXS, small-angle X-ray scattering; TEM, transmission electron microscopy; WAXS, wide-angle X-ray scattering.

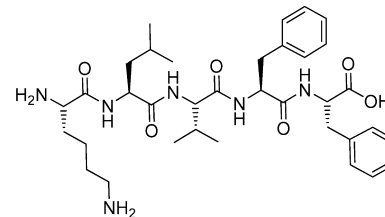
fibrillizes. In a separate study, fibril formation has been reported for the heptapeptide A β (16–22), ($\text{CH}_3\text{CO}-$)-KLVFFAE(–NH₂) (16). It has been suggested that fibrils of this peptide actually comprise nanotubes based on electron microscopy, atomic force microscopy, and small-angle scattering data (22). Analysis of the 3D structure of A β 42 from nuclear magnetic resonance (NMR) indicates that residues 18–26 form a β sheet as do residues 31–42 within the overall β -strand–turn– β -strand structure of residues 18–42 (residues 1–17 are disordered) (23). The sequence A β (17–23), which seems to be vital in amyloid self-assembly, has also been shown to be important in forming the correct β -pleated sheet structure of the A β peptide (8, 9). Computer modeling based on the calculation of partition functions of β -sheet peptide configurations predicts that A β (17–21) should be prone to β -sheet aggregation (17, 18). Algorithms based on the analysis of the aggregation properties of the constituent amino acids also predict aggregation for this region of A β (1–42) (19). Different methods to predict secondary structure indeed lead to different predictions for the conformation of KLVFF (24). The method of Garnier predicts α helices for KLVFF, whereas the Chou–Fasman method predicts that residues KLV are in β -strand structures and FF in α -helix structures.

In the present paper, we study self-assembly of KLVFF in dilute aqueous solution via CD, UV, and FTIR spectroscopy. We were motivated to address some of the conflicting reports in the literature discussed above. The combination of spectroscopic characterization methods provides a picture of β -sheet self-assembly at sufficiently high concentrations. At lower concentrations, CD and UV spectroscopy suggest the absence of a well-defined β -sheet conformation. However, the spectra point to aggregates in which there is a significant contribution from aromatic interactions of the F residues, in addition to the electrostatic interactions that result from the charge on the K residue. Confirmation of β -sheet self-assembly for dried samples is provided by fiber X-ray diffraction. Cryogenic transmission electron microscopy (cryo-TEM) provides direct, *in situ*, evidence for the formation of well-defined fibrils of large persistence length. Our cryo-TEM study is one of the first on this type of peptide fragment. There are significant differences in the morphology revealed by cryo-TEM and conventional TEM on dried and negatively stained samples, which are discussed in the context of the literature on amyloid peptide fragments. We also discuss the formation of hydrogels by KLVFF in more concentrated aqueous solution. We are not aware of prior papers on gelation of amyloid peptide fragments. The dynamic mechanical properties of the gels are probed by dynamic shear rheometry, and structural aspects are elucidated by light scattering and small-angle X-ray scattering (SAXS).

MATERIALS AND METHODS

Materials. KLVFF (Scheme 1) was synthesized by solid-phase synthesis techniques. Standard FastMoc [9-fluorenylmethyloxycarbonyl (Fmoc)-protecting group and activation by 2-(1*H*-benzotriazol-1-yl)-1,1,3,3-tetramethyluronium hexafluorophosphate (HBTU)] chemistry was used. Amino acids (Fmoc–lysine(Boc)–OH, Fmoc–leucine–OH, Fmoc–valine–OH, Fmoc–phenylalanine–OH), Fmoc–phenylalanine–

Scheme 1: Molecular Structure of KLVFF



Wang resin, and HBTU were purchased from Novabiochem (U.K.). HOEt/DMF (mixture of 1-hydroxybenzotriazole and dimethylformamide), DIEA/NMP (mixture of diisopropylethylamine and *N*-methylpyrrolidone), and NMP were obtained from Applied Biosystems (U.K.). Water (HPLC grade), acetonitrile (HPLC grade), and diethyl ether were purchased from Fluka (U.K.). Piperidine, trifluoroacetic acid (TFA), triisopropylsilane, methanol, and all other reagents were purchased from Sigma-Aldrich (U.K.) and were of the highest purity.

The peptide was synthesized on a 0.25 mmol scale using a fully automated peptide synthesizer (433A Applied Biosystems, U.K.), which allowed for direct conductivity monitoring of Fmoc deprotection.

The resin used was Fmoc–phenylalanine–Wang resin with 0.74 mmol/g substitution. The peptide was assembled from the C terminus toward the N terminus and was attached to the solid support at the C terminus by the α -carboxyl group of the amino acid. According to the standard FastMoc protocol, the first step of the reaction was to remove the Fmoc-protecting group from the amino acid using a solution of piperidine in NMP. The next step was activation of the carbonyl group of the new amino acid (dissolved in NMP) using HBTU (dissolved in HOEt, DIEA, and DMF). The activated amino acid was transferred from the activation vessel to the reaction vessel containing the previously deprotected amino terminus of the built peptide chain, and coupling was performed. To obtain the highest coupling efficiency, a 4 times excess of each amino acid was used in 0.25 mmol cycles. Peptide attached to the solid support was obtained from the synthesizer. In the cleavage step, a mixture of 95% TFA, 2.5% triisopropylsilane, and 2.5% water was used. The sample was occasionally shaken at room temperature for approximately 4 h, and the insoluble resin was washed with TFA. The peptide solution was precipitated in ice-cold diethyl ether, and the precipitant was separated by centrifugation. The solid peptide was washed with diethyl ether and dried. During the cleavage, the side-chain-protecting group (Boc) was removed by TFA. The crude peptide was purified by reverse-phase high-performance liquid chromatography (RP-HPLC; Beckman System Gold with Programmable Solvent Module 126 and Diode Array Detector Module 168) using a C18 preparative column (Supelco), for 30 min with flow rates of 2.5 mL/min. A mobile phase of water with 0.1% TFA and acetonitrile with 0.1% TFA was used. Sample elution was monitored using a UV-vis detector operating at 210 and 254 nm. The purity of the sample was monitored on an analytical column (C18, Vydac) and was $\geq 95\%$. The sample dissolved in HPLC solvents was freeze-dried. The molecular weight was determined by electrospray ionization (ESI) mass spectroscopy.

ESI mass spectroscopy provided (*m/z*): 653.41 [expected: 653.4].

Proton NMR spectra in DMSO were measured on a Bruker AMX 400 spectrometer. Unambiguous assignments of proton shifts were made by comparing with homo- and heteronuclear correlation spectra (COSY, HETCOR, and TOCSY).

The KLVFF ^1H NMR (400 MHz DMSO, ppm): 0.71 [2d, 6H, 2 \times CH₃ (Val) $J = 4.2$ Hz], 0.84 [2d, 6H, 2 \times CH₃ (Leu) $J = 6.52$ Hz], 1.24–1.72 [m, 9H, 4 \times CH₂ (Lys, Leu) CH (Leu)], 1.85 [m, 1H, CH (Val)], 2.68–2.77 [m, 2H, CH₂ (Lys)], 2.87–3.08 [m, 4H, 2 \times CH₂ (Phe)], 3.74–3.82 [m, 1H, CH(α) (Lys)], 4.11[dd, 1H, CH(α) (Val) $J_1 = 7.38$ Hz, $J_2 = 8.96$ Hz], 4.37–4.61[m, 3H, CH(α), (Leu, Phe)], 7.11–7.28 [m, 10H, arom. (Phe)], 7.85 [s, 2H, NH₂ (Lys)], 7.91–7.98 [m, 2H, 2 \times NH (Val, Phe)], 8.16 [s, 2H, NH₂ (Lys)], 8.23 [d, 1H, NH (Phe) $J = 7.7$ Hz], 8.49 [d, 1H, NH (Leu) $J = 7.93$ Hz].

The KLVFF ^{13}C NMR (100 MHz DMSO, ppm): 18.0, 19.2 [2C, 2 \times CH₃ (Val)], 20.9 [1C, CH₂ (Lys)], 21.6, 23.1 [2C, 2 \times CH₃ (Leu)], 24.0 [1C, CH (Leu)], 26.4 [1C, CH₂ (Lys)], 30.5 [1C, CH₂ (Lys)], 30.7 [1C, CH (Val)], 36.7, 37.6 [2C, 2 \times CH₂ (Phe)], 38.5 [1C, CH₂ (Lys)], 40.5 [1C, CH₂ (Leu)], 51.2 [1C, CH(α) (Leu)], 51.7 [1C, CH(α) (Lys)], 53.3, 53.4 [2C, CH(α) (Phe)], 57.6 [1C, CH(α) (Val)], 126.2, 126.5, 128.0, 128.2, 129.1 [10C, arom. (Phe)], 137.3, 137.6 [2C, arom. (Phe)], 168.2, 170.4, 170.9, 171.3, 172.6 [5C, CO (Lys, Leu, Val, Phe)].

Circular Dichroism. The CD spectra were recorded on a Chirascan spectropolarimeter (Applied Photophysics, U.K.). Samples were dissolved in water (0.03 wt %), PBS (0.03 wt %), and trifluoroethanol (TFE) (0.018 and 0.036 wt %) and loaded into a 1 mm quartz cuvette. Spectra were obtained from 190 to 250 nm with a 0.5 nm step, 1 nm bandwidth, and 2 s collection time per step at 20 °C, taking five averages.

UV Fluorescence Spectroscopy. Spectra were measured on a Perkin Elementar Luminescence spectrometer LS50B. Samples were contained in 1.0 cm path-length quartz cuvettes. The fluorescence intensity was measured for water and KLVFF (0.000 003 wt %, the maximum concentration for reliable UV transmission) in water by excitation at 265 nm (slit width of 5 nm). The spectra were recorded from 280 to 500 nm, taking 20 averages at room temperature, and the background was subtracted.

Fourier Transform Infrared Spectroscopy. FTIR spectra including amide bands were recorded on a Nicolet FTIR Nexus spectrometer equipped with a DTGS detector. The KLVFF solution in PBS at pH 7.4 (1 and 3 wt %) and in D₂O (3 wt %) was sandwiched between two CaF₂ plate windows (spacer 0.006 mm), and a solid film of dry peptide was deposited on one CaF₂ plate by drying the same solution. The solution in PBS (3 wt %) formed a gel after 30 min of incubation. Spectra were scanned 64 times over the range of 4000–400 cm⁻¹. Spectral Manager for Windows was used for data acquisition and handling.

X-Ray Diffraction. X-ray diffraction was performed on stalks prepared by drying filaments of the peptide. Aqueous solution (3 wt %) of peptide was suspended between the ends of wax-coated capillaries and dried (25). The stalks were mounted (vertically) onto the goniometer of an Oxford Instruments Gemini X-ray diffractometer.

Electron Microscopy. Cryo-TEM, performed at the University of Delaware, is a powerful technique to elucidate the self-assembled structure of amphiphilic molecules in solution (26). A thin film (\sim 100 nm) of the 3 wt % KLVFF sample

in water, heated at 60 °C for 10 min, was transferred to a lacey carbon grid, blotted with filter paper, and plunged into liquid ethane. All samples were prepared using the environmentally controlled, automated Vitrobot from the FEI Company, Hillsboro, OR. In a typical sample preparation, the sample chamber was maintained at 25 °C and 40–50% relative humidity. Prior to plunging in liquid ethane, the sample was blotted with a filter paper once for 1 s. After vitrification, the samples were transferred to a Gatan cryo-holder precooled to –175 °C, before inserting into the electron microscope. Imaging was carried out in bright field mode at 120 kV in a Technai T12 electron microscope (FEI Company, Hillsboro, OR). During imaging, the temperature of the sample holder was maintained at –175 °C to inhibit sublimation of vitreous water.

Small-Angle X-ray Scattering. SAXS experiments were performed on beamline ID02 at the European Synchrotron Radiation Facility, Grenoble, France. Samples were placed in sealed cells in an O ring between mica windows. Temperature control was achieved using a Peltier device. A CCD detector was used to collect two-dimensional images, which were reduced by radial integration to one-dimensional profiles. The sample–detector distance was 2 m. Subtraction of background scattering using a water reference was performed for the data presented here.

Static Light Scattering (SLS). Static light scattering was performed using a custom built instrument described elsewhere (27). Briefly, it comprises a He–Ne laser, optics train, sample contained in a Linkam CSS 450 shear cell, a diffuser plate, and a CCD camera to detect images. The sample was subjected to a range of shear rates; however, no significant orientation was observed, and therefore, the two-dimensional patterns obtained were integrated to one-dimensional profiles of intensity versus scattering angle and hence wavenumber q (calibrated using a diffraction grating). No systematic variation in one-dimensional profiles with shear conditions was observed, and therefore, data are plotted together.

Rheology. Rheological properties were determined using a controlled stress TA Instruments AR-2000 rheometer (TA Instruments). A cone-and-plate geometry (cone diameter, 20 mm; angle, 1°) was used. Time sweeps were recorded at 10 and 25 °C (angular frequency $\omega = 10$ rad s⁻¹). Temperature scans were performed within the range of 20–50 °C at a heating rate 1 °C min⁻¹, with the instrument in oscillatory mode at an angular frequency $\omega = 10$ rad s⁻¹. Frequency sweeps were performed at 25 °C. Preliminary strain sweeps were performed for each sample to define the linear viscoelastic region, thus ensuring that moduli were independent of strain.

RESULTS AND DISCUSSION

Secondary Structure. The secondary structure of peptide KLVFF was assessed using CD for dilute solutions and FTIR and Raman spectroscopy for concentrated solutions and gels. UV absorption and fluorescence spectroscopy were used to probe π – π^* stacking interactions.

Figure 1 shows CD data for KLVFF in aqueous solutions and also in trifluoroethanol. It has been observed that CD spectra of short peptides in which self-assembly in very dilute solution is driven by stacking interactions of aromatic units show positive maxima at 200 and 218 nm, in contrast to the

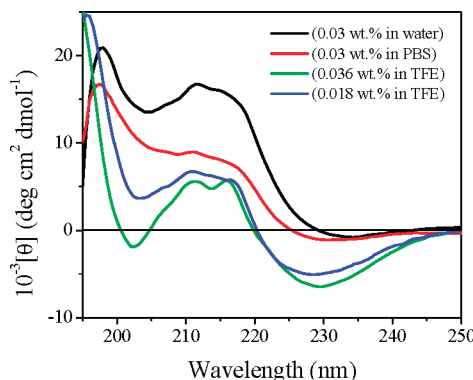


FIGURE 1: CD spectra of KLVFF in water (0.03 wt %), PBS (0.03 wt %), and TFE (0.018 and 0.036 wt %).

usual negative maximum for β sheets observed at approximately 216 nm (28). For example, this has been observed for a diphenylalanine-based dipeptide (29) or in our own study on FFKLVFF in methanol and TFE (30). The peak at 200 nm is associated with a $\pi-\pi^*$ transition, and the peak at 217 nm is associated with a $n-\pi^*$ transition (29). The CD spectrum obtained for KLVFF in water seems to be dominated by a positive maximum at 198 nm, although there is an extended peak in the range of 210–220 nm. The positive maxima in pH 7.4 PBS solution correspond closely to those observed in water. For KLVFF in TFE, the lower wavelength peak is shifted to 196 nm (well-resolved for 0.018 wt %) and the higher wavelength broad peak splits into two peaks at 212 and 217 nm (well-resolved for 0.036 wt %). For the TFE spectra, we observe that the negative maxima at 228 nm are deeper than for the aqueous solvents. These results are distinct to those previously reported for AcNH–KLVFF–CONH₂ and the closely related peptide NH₂–KLVFFAE–CONH₂ (in a similar concentration range) (14, 15). The reported spectra in the range of 200–250 nm show decreasingly negative ellipticity in the range of 200–220 nm followed by a plateau with several shallow minima and maxima. It appears that the N-terminal acetylation and C-terminal amidation has a significant impact on the self-assembly. In our peptide NH₂–KLVFF–COOH, the presence of two charged terminal groups enables self-assembly into better defined aggregates in which interactions of F units lead to identifiable features in the CD spectra. This points to the important role of both electrostatic interactions and aromatic interactions in the self-assembly process. The CD spectra were obtained approximately 1 day after preparation of the solutions; therefore, the samples should be well-equilibrated. We have not, however, attempted to study the kinetics of self-assembly by monitoring the development of the CD spectrum.

As further tools to probe $\pi-\pi^*$ stacking interactions of aromatic units, UV-visible fluorescence (Figure 2) and absorption (Figure S1 in the Supporting Information) spectroscopy were used to investigate low-concentration aqueous solutions. The fluorescence spectrum exhibits a peak at 313 nm, which corresponds to $\pi-\pi^*$ stacking interactions of phenyl units. In the absorption spectrum, two peaks occur at 210 and 260 nm, with the latter corresponding to that previously reported for F residues in proteins (31, 32). The importance of aromatic stacking interactions in the formation of certain amyloid fibrils has been highlighted by several groups, as reviewed elsewhere (6), and our results provide

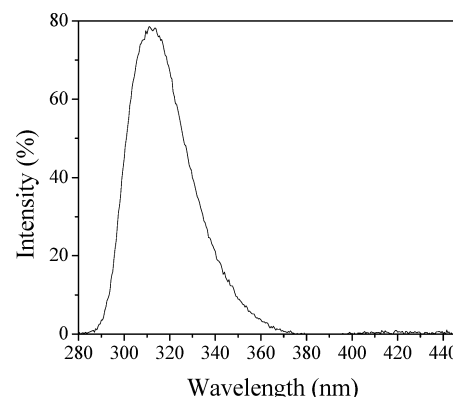


FIGURE 2: UV fluorescence spectra showing aromatic interactions in KLVFF (0.000 003 wt % in water).

further evidence on the importance of such interactions in dilute solution of KLVFF.

The main focus of the FTIR experiments was on the amide I band, which is sensitive to secondary structure. Figure 3a contains spectra for a 1 wt % solution and a specimen dried from a 1 wt % solution in PBS. Figure 3b shows spectra for 3 wt % solutions in PBS and water and a specimen dried from a 3 wt % solution in water. An expanded spectrum of a dried specimen (from a 3 wt % solution) together with a Raman spectrum for a dried sample are included in Figure S2 in the Supporting Information.

In the spectra in Figure 3, the peaks at 1629 cm⁻¹ are certainly associated with a β -sheet structure (33–37). Peaks at 1643–1648 cm⁻¹ may be assigned to random-coil or unordered structures (35–38). Peaks at 1673–1680 cm⁻¹ are often associated with an antiparallel β -sheet structure (37), although there is controversy in the literature on this (39). Model calculations of amide I frequencies for globular proteins indicate that a band in this region is not a reliable indicator of antiparallel β sheets (40). In addition, several reports assign bands in this region to other structures, including parallel β sheets (33), bends, or turns (35, 37). The observation of the 1675–1680 cm⁻¹ peak may also depend upon whether the β sheet is finite (39). For this reason, our discussion focuses on the relative intensity of the “unambiguous” 1629 cm⁻¹ β -sheet feature relative to the other peaks. From parts a and b of Figure 3, we observe that the 1629 cm⁻¹ β -sheet peak becomes relatively much more intense in the dried sample and that the spectra for the dried sample are similar whether the specimen was dried from 1 or 3 wt % solution. The spectra for solutions contain peaks from other secondary structures that may be disordered or turn structures. Considering the role of the concentration, the 1629 cm⁻¹ peak is relatively much more intense for the 3 wt % PBS solution than the 1 wt % PBS solution. Finally, considering the effect of buffer, the 1629 cm⁻¹ peak is much stronger in PBS than in D₂O (data for 3 wt % sample); however, it has to be considered that the 3 wt % PBS solution is a gel (*vide infra*), whereas the 3 wt % aqueous solution is still fluid. The first two observations point to the role of the concentration in the self-assembly process. It appears that β -sheet self-assembly is strongly promoted by an increase in the concentration, in particular in the range of 1–3 wt %, and increases further upon drying (100% concentration). The third observation points to the role of electrostatic interactions in the self-assembly process. Screening the charge on

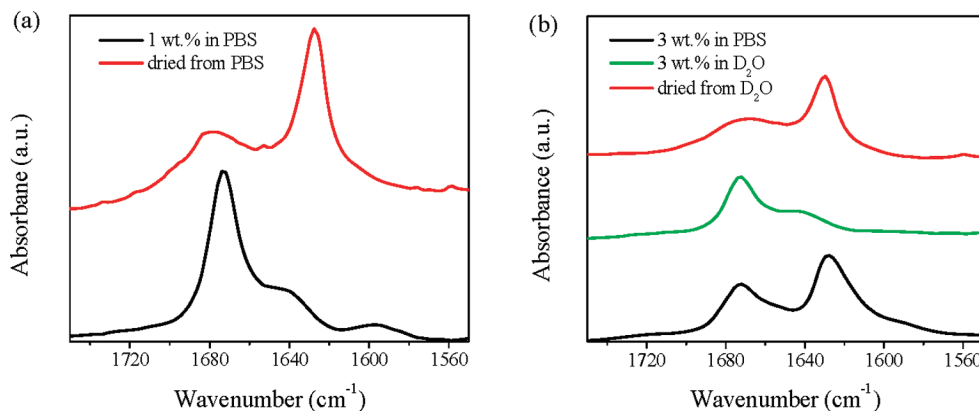


FIGURE 3: (a) FTIR spectra in the amide I region for 1 wt % KLVFF in PBS in solution and dried. (b) FTIR spectra in the amide I region for 3 wt % KLVFF in PBS in solution, 3 wt % in D_2O and dried.

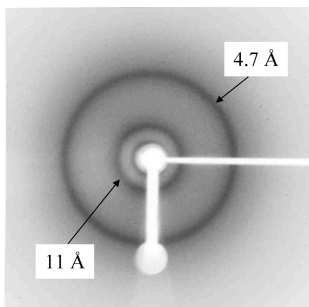


FIGURE 4: X-ray diffraction pattern from a dried stalk. The shadow of the sample is visible in the lower part of the image. The horizontal white line is the beamstop.

$NH_2-KLVFF-COOH$ (net positive charge at pH 7 because of the lysine residue) in buffer solution leads to an increase in the intensity of the 1629 cm^{-1} peak associated with β sheets.

In summary, FTIR (supported by Raman spectroscopy) indicates a β -sheet structure in dried films and in a 3 wt % PBS gel, with some β -sheet character in more dilute solutions. The 1 wt % solutions contain substantial contributions from unordered or β -turn structures. CD, UV absorption, and fluorescence spectra are dominated by aromatic interactions in dilute solution. The CD spectrum in dilute solution is not that expected for a β sheet (negative maximum at 216 nm). This may be due to the low concentrations used in the CD experiments, which may be below the critical aggregation concentration for the peptide. It is possible that at low concentrations the peptide is aggregated such that the hydrophobic domains, especially F residues, are sequestered from water, but that a β -sheet structure has not fully developed.

Surprisingly, KLVFF did not exhibit binding of thioflavin T (another typical test for amyloid formation), as probed by UV/vis fluorescence and as reported previously for KLVFF in aqueous buffer solution (12).

X-ray diffraction was also used to probe secondary structure in dried stalks (prepared by drying a thread of concentrated solution between the ends of two waxed capillaries). The X-ray diffraction pattern shown in Figure 4 exhibits powder rings from an unoriented “cross- β ” pattern, which confirms a β -sheet structure for the dried sample (6). The corresponding Bragg spacings $d = 4.7$ and 11 \AA arise from the peptide backbone separation within a β strand and the β -sheet spacing due to side-chain packing.

Cryo-TEM provides clear support for self-assembly of KLVFF into well-defined fibrils. Figure 5 presents images obtained for a 3 wt % solution in water. Stiff fibrils several micrometers in length with an average diameter $d = 9.68 \pm 0.92\text{ nm}$ are evident. Figure 5b shows local alignment of fibrils, while Figure 5c shows a region of fibrillar bundles (left) coexisting with isolated fibrils (right). The fibril radius is larger than the length of KLVFF, which is 1.75 nm in a β strand. This indicates that the fibrils are formed from assemblies of individual β sheets, possibly twisted ribbons (41). However, in the absence of higher resolution, we do not have a detailed model at present.

The cryo-TEM images provide direct, *in situ* visualization of amyloid fibril formation, thus eliminating the artifacts induced in conventional TEM on dried and negatively stained samples. Figure S3 in the Supporting Information shows a typical image from such experiments. We believe that a comparison of the cryo-TEM results with the conventional TEM micrographs here suggests that drying effects may have a significant effect on the morphology imaged by negative-stain TEM.

Hydrogel Formation. Significant differences were observed in the association properties of solutions of KLVFF dissolved in PBS compared to water, at higher concentrations. KLVFF dissolved in water stays liquid up to 4.0 wt %, whereas in PBS, a gel forms at higher concentrations. Gelation takes approximately 15 h for a 2.5 wt % sample, decreasing to around 2 h for samples with concentrations 3.0–4.0 wt %. The observation of gelation for the sample in PBS is presumably due to the screening of electrostatic charges on the C and N termini in the buffer solution. KLVFF has a charge of +1 in pH 7 aqueous solution, arising from the lysine residue. The screening of the charge in buffer solution may enable the aggregation of peptide fibrils into a gelled network. The observation of a gel for the 3 wt % sample in PBS may contribute to the difference in FTIR spectra for the 3 wt % solutions in PBS or D_2O (Figure 3), in particular, the peak broadening observed in the PBS spectrum.

The gels formed were quite fragile. As shown in Figure 6, the initial gel (Figure 6a) could be broken up by, for example, vortex mixing, resulting in a viscous but flowing sample (Figure 6b). The network was rebuilt, leading to gelation after 30 min resting (Figure 6c).

To monitor the development of viscoelasticity of hydrogels, a 3 wt % solution in PBS was left to gel in a vial at room temperature and then transferred to the rheometer. The

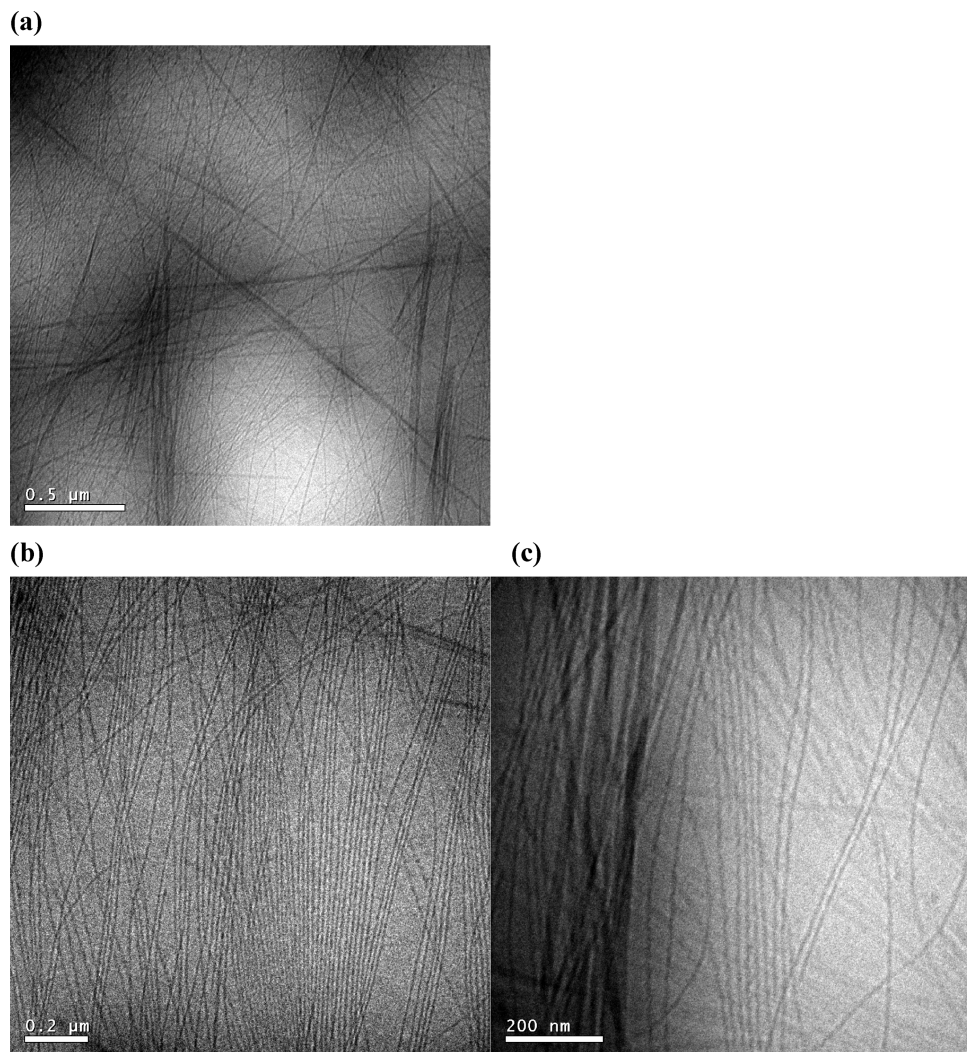


FIGURE 5: Cryo-TEM images from a 3 wt % solution of KLVFF in water.

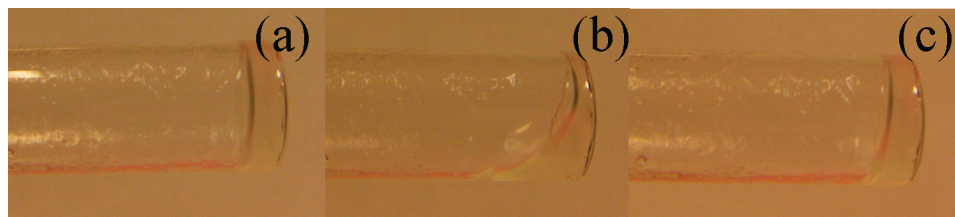


FIGURE 6: Images of 3 wt % KLVFF in PBS in a vial. (a) Gel prior to shearing, (b) fluid after 30 s of vortex mixing, and (c) reformed soft gel network after 30 min.

sample was preconditioned at 300 Pa for 30 s to destroy any possible network formation. The preconditioned sample was left to gel under isothermal conditions, while the complex viscosity η^* was monitored ($\omega = 10 \text{ rad s}^{-1}$, strain = 0.5%). The $\eta^*(t)$ curves thus obtained at $T = 10$ and 25 °C are presented in Figure 7. We note the higher initial η^* values and the more rapid development of viscoelasticity at 25 °C compared to 10 °C. At longer times, the viscosity η^* of the gel at 25 °C approached that at 10 °C. After a period of 4 h at either temperature, the samples had developed strong viscoelastic characteristics. A frequency sweep performed 90 min after the cessation of shearing (Figure 8) shows G' essentially independent of frequency, consistent with the development of a network. In another experiment (data not shown here), a gel was left to set at 20 °C and then a temperature ramp was performed. G' of the gel was found

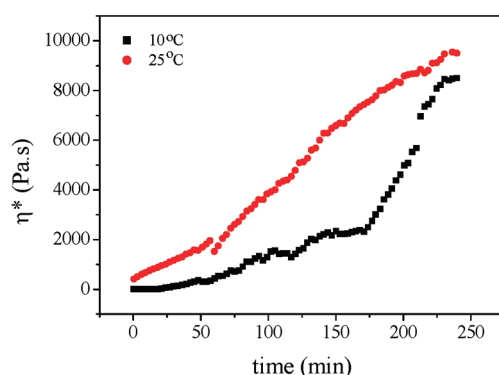


FIGURE 7: Development of complex viscosity versus time showing gelation of 3 wt % KLVFF in PBS. Conditions: $\omega = 10 \text{ rad s}^{-1}$, strain = 0.5%, temperatures indicated.

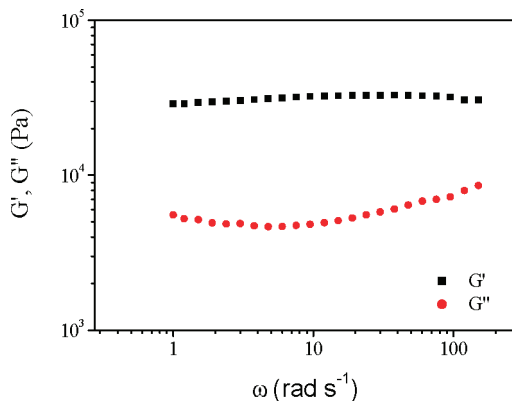


FIGURE 8: Frequency sweep performed at 25 °C after an ageing time of 90 min.

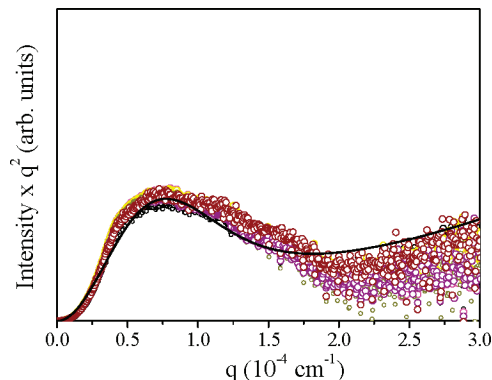


FIGURE 9: SLS data in Kratky representation (○). The spread in the data results from repeat runs under different shear conditions (no systematic trend as a function of the shear rate was observed). The solid line is a model fit described in the text.

to increase monotonically with temperature upon heating within the range of 20–50 °C. Finally, we note that a 1 wt % solution was found to exhibit a small but finite yield stress when aged in the rheometer for 5 h.

The structure of the PBS networks was probed by SLS and SAXS. Figure 9 shows SLS data presented in the form of a Kratky plot. Use of Kratky plots enables branched versus linear structures to be distinguished. There is a characteristic maximum in intensity in a Kratky plot for a branched structure. Figure 9 also contains a fit to a form factor of a branched wormlike chain structure, motivated by prior work by Pallitto et al., who have applied linear and branched wormlike chain models to describe SLS data from $\text{A}\beta$ alone and also from mixtures of $\text{A}\beta$ with $\text{A}\beta$ fragments [including $\text{A}\beta(16–20)$] (42). Because a clear maximum is observed in the data for the KLVFF solution in PBS (Figure 9), we used the branched wormlike chain form factor previously reported (42, 43). The fit is satisfactory and provides dimensions for the fibrillar strand structure in the gel, in particular, a branch contour length $L_c = 8 \mu\text{m}$, a Kuhn length $l_K = 2 \mu\text{m}$, and a network branch functionality $f = 7$. The length parameters are significantly larger than those previously reported for the full 39 residue $\text{A}\beta$ peptide (42). This may reflect the much higher concentration used in the present study (3 versus 5×10^{-4} wt %), even though the current peptide is shorter. The contour length obtained is, however, consistent with the cryo-TEM images in Figure 5, which show extended fibrils with a contour length of at least several micrometers.

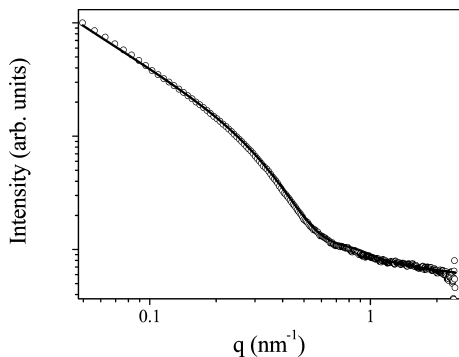


FIGURE 10: SAXS data (○) for KLVFF (3 wt % PBS solution) measured at 70 °C, with a model fit (—) to the polydisperse cylinder form factor.

SAXS was used to probe the structure in the PBS gel at much shorter length scales, corresponding to the local β -sheet fibril structure. SAXS offers the advantage, similar to cryo-TEM, that the structure can be probed *in situ* without any artifacts from drying. Figure 10 shows data obtained at 70 °C. The data can be fitted using the form factor of a thin cylinder used by us previously to fit SAXS data for related peptide FFKLFFF (30). Details of the model used are provided in the Supporting Information. The resulting fibril radius is 5.8 nm, with 8% polydispersity. These dimensions are in excellent agreement with those extracted from cryo-TEM measurements (diameter $d = 9.68 \pm 0.92 \text{ nm}$). The SAXS data at 20 °C (not shown) could not be fitted to a cylinder form factor. This suggests possibly a coexistence of aggregates with different shape in the solution; however, unfortunately, it did not prove possible to uniquely model the low-temperature SAXS data. It appears that incubation of the sample is required to produce well-defined fibrils.

SUMMARY

The self-assembly of a fragment of the $\text{A}\beta$ peptide, $\text{A}\beta(16–20) \text{ NH}_2\text{--KLVFF--COOH}$, has been studied in aqueous solution. In very dilute solution, aromatic interactions play a major role in driving self-assembly as probed by UV spectroscopy and CD. FTIR confirms the presence of β -sheet features at higher concentrations, although other structures are certainly present. In more concentrated solution, β -sheet fibrils predominate as confirmed by the combination of FTIR, cryo-TEM, and SAXS. The fibril dimensions obtained from cryo-TEM and SAXS are in very good agreement and provides clear evidence that fibrils are formed in aqueous solution. This helps to resolve some contradictory reports in the literature on KLVFF fibrillization. A further key finding of our work is the role of sample preparation method, i.e., drying of films, in modifying the self-assembly process. Conventional TEM on negatively stained and dried films does not clearly reveal fibrils, in contrast to cryo-TEM. The mixture of fibrillar and globular aggregates observed is similar to prior reports of amyloid “proto-fibrils”, but the structures observed by conventional TEM may result from or be significantly perturbed by the drying process. FTIR and Raman spectroscopy also reveal large changes when comparing spectra for solutions or dried films. In particular, the 1629 cm^{-1} amide I FTIR peak is relatively more intense for dried films.

In more concentrated (3 wt %) PBS solution, hydrogel formation was observed and the rheology was subjected to

preliminary analysis. The hydrogel results from the formation of a fibrillar network, as confirmed by SAXS and SLS. Hydrogel formation was not observed for a water solution at the same concentration, and hydrogelation in PBS may therefore result from the screening of electrostatic interactions on the cationic KLVFF peptides by the buffer salts. Our results indicate that self-assembly of KLVFF is controlled by a combination of aromatic stacking interactions of phenylalanine residues and electrostatic interactions from lysine and the terminal units.

ACKNOWLEDGMENT

We thank Chris Stain and Peter Harris (Centre for Advanced Microscopy, University of Reading) for assistance with the negative-stain TEM experiments, Yu Gan and Adam Squires for help with XRD and preparation of stalks, and Luke Clifton for assistance with FTIR. We are grateful to Dr. T. Narayanan for assistance with SAXS experiments at the ESRF, France.

SUPPORTING INFORMATION AVAILABLE

UV/vis absorption spectroscopy, full FTIR and Raman spectra, negative-stain TEM, and SAXS. This material is available free of charge via the Internet at <http://pubs.acs.org>.

REFERENCES

- Teplow, D. B. (1998) Structural and kinetic features of amyloid β -protein fibrillogenesis. *Amyloid* 5, 121–142.
- Goedert, M., and Spillantini, M. G. (2006) A century of Alzheimer's disease. *Science* 314, 777–781.
- Roberson, E. D., and Mucke, L. (2006) 100 years and counting: Prospects for defeating Alzheimer's disease. *Science* 314, 781–784.
- Sipe, J. D. (1992) Amyloidosis. *Annu. Rev. Biochem.* 61, 947–975.
- Caughey, B., and Lansbury, P. T. (2003) Protofibrils, pores, fibrils, and neurodegeneration: Separating the responsible protein aggregates from the innocent bystanders. *Annu. Rev. Neurosci.* 26, 267–298.
- Hamley, I. W. (2007) Peptide Fibrillisation. *Angew. Chem., Int. Ed.* 46, 8128–8147.
- Serpell, L. C. (2000) Alzheimer's amyloid fibrils: Structure and assembly. *Biochim. Biophys. Acta* 1502, 16–30.
- Hilbich, C., Kisterswoijke, B., Reed, J., Masters, C. L., and Beyreuther, K. (1992) Substitutions of hydrophobic amino acids reduce the amyloidogenicity of Alzheimer's disease β -A4 peptides. *J. Mol. Biol.* 228 (2), 460–473.
- Wood, S. J., Wetzel, R., Martin, J. D., and Hurle, M. R. (1995) Prolines and amyloidogenicity in fragments of the Alzheimer's peptide β A4. *Biochemistry* 34 (3), 724–730.
- Tjernberg, L. O., Naslund, J., Lindqvist, F., Johansson, J., Karlstrom, A. R., Thyberg, J., Terenius, L., and Nordstedt, C. (1996) Arrest of β -amyloid fibril formation by a pentapeptide ligand. *J. Biol. Chem.* 271 (15), 8545–8548.
- Tjernberg, L. O., Lilliehook, C., Callaway, D. J. E., Naslund, J., Hahne, S., Thyberg, J., Terenius, L., and Nordstedt, C. (1997) Controlling amyloid β -peptide fibril formation with protease-stable ligands. *J. Biol. Chem.* 272 (19), 12601–12605.
- Tjernberg, L. O., Callaway, D. J. E., Tjernberg, A., Hahne, S., Lilliehöök, C., Terenius, L., Thyberg, J., and Nordstedt, C. (1999) A molecular model of Alzheimer amyloid β -peptide fibril formation. *J. Biol. Chem.* 274 (18), 12619–12625.
- Findeis, M. A., Musso, G. M., Arico-Muendel, C. C., Benjamin, H. W., Hundal, A. M., Lee, J. J., Chin, J., Kelley, M., Wakefield, J., Hayward, N. J., and Molineaux, S. M. (1999) Modified-peptide inhibitors of amyloid β -peptide polymerization. *Biochemistry* 38 (21), 6791–6800.
- Gordon, D. J., Sciarretta, K. L., and Meredith, S. C. (2001) Inhibition of β -amyloid(40) fibrillogenesis and disassembly of β -amyloid(40) fibrils by short β -amyloid congeners containing *N*-methyl amino acids at alternate residues. *Biochemistry* 40, 8237–8245.
- Gordon, D. J., Tappe, R., and Meredith, S. C. (2002) Design and characterization of a membrane permeable *N*-methyl amino acid-containing peptide that inhibits $\text{A}\beta$ 1–40 fibrillogenesis. *J. Pept. Res.* 60, 37–55.
- Balbach, J. J., Ishii, Y., Antzutkin, O. N., Leapman, R. D., Rizzo, N. W., Dyda, F., Reed, J., and Tycko, R. (2000) Amyloid fibril formation by $\text{A}\beta$ 16–22, a seven-residue fragment of the Alzheimer's β -amyloid peptide, and structural characterization by solid state NMR. *Biochemistry* 39, 13748–13759.
- Fernandez-Escamilla, A.-M., Rousseau, F., Schymkowitz, J., and Serrano, L. (2004) Prediction of sequence-dependent and mutational effects on the aggregation of peptides and proteins. *Nat. Biotechnol.* 22 (10), 1302–1306.
- Rousseau, F., Schymkowitz, J., and Serrano, L. (2006) Protein aggregation and amyloidosis: Confusion of the kinds. *Curr. Opin. Struct. Biol.* 16, 118–126.
- Pawar, A. P., DuBay, K. F., Zurdo, J., Chiti, F., Vendruscolo, M., and Dobson, C. M. (2005) Prediction of "aggregation-prone" and "aggregation-susceptible" regions in proteins associated with neurodegenerative disease. *J. Mol. Biol.* 350, 379–392.
- Kallberg, Y., Gustafsson, M., Persson, B., Thyberg, J., and Johansson, J. (2001) Prediction of amyloid fibril-forming proteins. *J. Biol. Chem.* 276 (16), 12945–12950.
- Zhang, G., Leibowitz, M. J., Sinko, P. J., and Stein, S. (2003) Multiple-peptide conjugates for binding β -amyloid plaques of Alzheimer's disease. *Bioconjugate Chem.* 14, 86–92.
- Lu, K., Jacob, J., Thiagarajan, P., Conticello, V. P., and Lynn, D. G. (2003) Exploiting amyloid fibril lamination for nanotube self assembly. *J. Am. Chem. Soc.* 125, 6391–6393.
- Lührs, T., Ritter, C., Adrian, M., Riek-Loher, D., Bohrmann, B., Döbeli, H., Schubert, D., and Riek, R. (2005) 3D structure of Alzheimer's amyloid- β (1–42) fibrils. *Proc. Natl. Acad. Sci. U.S.A.* 102 (48), 17342–17347.
- Malinchik, S. B., Inouye, H., Szumowski, K. E., and Kirschner, D. A. (1998) Structural analysis of Alzheimer's β (1–40) amyloid: Protofilament assembly of tubular fibrils. *Biophys. J.* 74, 537–545.
- Makin, O. S., and Serpell, L. C. (2004) The structure of amyloid. *Fibre Diffr. Rev.* 12, 29–35.
- Cui, H., Hodgdon, T. K., Kaler, E. W., Abezgaous, L., Danino, D., Lubovsky, M., Talmon, Y., and Pochan, D. J. (2007) Elucidating the assembled structure of amphiphiles in solution via cryogenic-transmission electron microscopy. *Soft Matter* 3, 945–955.
- Castelletto, V., and Hamley, I. W. (2006) Capillary flow behaviour of worm-like micelles studied by small angle X-ray scattering and small angle light scattering. *Polym. Adv. Technol.* 17 (3), 137–144.
- Woody, R. W. (1994) Circular dichroism of peptides and proteins, in *Circular Dichroism. Principles and Applications* (Nakanishi, K., Berova, N., and Woody, R. W., Eds.) pp 473–496, VCH, New York.
- Gupta, M., Bagaria, A., Mishra, A., Mathur, P., Basu, A., Ramakumar, S., and Chauhan, V. S. (2007) Self-assembly of a dipeptide-containing conformationally restricted dehydrophenylalanine residue to form ordered nanotubes. *Adv. Mater.* 19, 858–861.
- Krysman, M. J., Castelletto, V., and Hamley, I. W. (2007) Fibrillation of hydrophobically modified amyloid peptide fragments in an organic solvent. *Soft Matter* 3, 1401–1406.
- Kitagawa, T. (1992) Investigation of higher order structures of proteins by ultraviolet resonance Raman spectroscopy. *Prog. Biophys. Mol. Biol.* 58, 1–18.
- Schmid, F. X. (2001) Macromolecular interactions: UV-visible spectrophotometry, in *Encyclopedia of Life Sciences*, Nature Publishing, London, U.K.
- Susi, H., and Byler, D. M. (1987) Fourier transform infrared study of proteins with parallel β -chains. *Arch. Biochem. Biophys.* 258 (2), 465–469.
- Haris, P., and Chapman, D. (1995) The conformational analysis of peptide using Fourier transform IR spectroscopy. *Biopolymers* 37, 251–263.
- Stuart, B. (1997) *Biological Applications of Infrared Spectroscopy*, Wiley, Chichester, U.K.
- Jackson, M., and Mantsch, H. H. (1995) The use and misuse of FTIR spectroscopy in the determination of protein structure. *Crit. Rev. Biochem. Mol. Biol.* 30 (2), 95–120.

37. Pelton, J. T., and McLean, L. R. (2000) Spectroscopic methods for analysis of protein secondary structure. *Anal. Biochem.* 277, 167–176.
38. Surewicz, W. K., and Mantsch, H. H. (1988) New insight into protein secondary structure from resolution-enhanced infrared spectra. *Biochem. Biophys. Acta* 952, 115–130.
39. Barth, A., and Zscherp, C. (2002) What vibrations tell us about proteins. *Q. Rev. Biophys.* 35 (4), 369–430.
40. Torii, H., and Tasumi, M. (1992) Model calculations on the amide-I infrared bands of globular proteins. *J. Chem. Phys.* 96 (5), 3379–3387.
41. Aggeli, A., Nyrkova, I. A., Bell, M., Harding, R., Carrick, L., McLeish, T. C. B., Semenov, A. N., and Boden, N. (2001) Hierarchical self-assembly of chiral rod-like molecules as a model for peptide β -sheet tapes, ribbons, fibrils and fibres. *Proc. Natl. Acad. Sci. U.S.A.* 98 (21), 11857–11862.
42. Pallitto, M. M., Ghanta, J., Heinzelman, P., Kiessling, L. L., and Murphy, R. M. (1999) Recognition sequence design for peptidyl modulators of β -amyloid aggregation and toxicity. *Biochemistry* 38, 3570–3578.
43. Shen, C.-L., Fitzgerald, M. C., and Murphy, R. M. (1994) Effect of acid predissolution on fibril size and fibril flexibility of synthetic β -amyloid peptide. *Biophys. J.* 67, 1238–1246.

BI8000616